KRONOS FUSION ENERGY

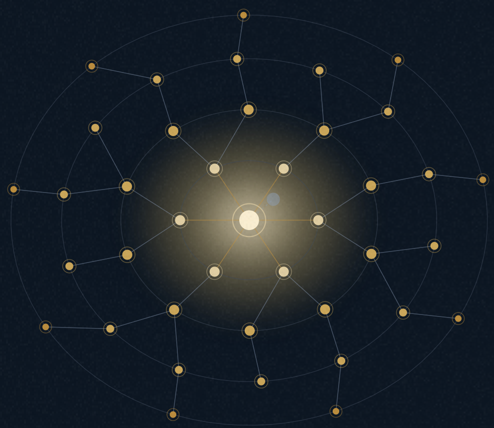

PAPER 2.51 · THE KRONOS 2026 SERIES

A Machine-Learning Interatomic-Potential to Activation-Transport Pipeline for Low-Activation Fusion Alloy Discovery: CHGNet Screening, DFT Confirmation, and OpenMC/FISPACT Down-Selection

Selecting a plasma-facing structural alloy for a fusion power plant is a search through a combinatorial composition space against two filters a human cannot apply by hand:...

Read it live — 3-D model · physics validator · film series

BY P I FORD

2026 · EDITORIAL EDITION

THE OFFICIAL RECORD

What this document is, and how to read its numbers

This is a combined editorial. It gathers, in one volume, the two design studies Kronos Fusion Energy released in 2026 — a compact spherical-tokamak tritium/helium-3 breeder and a deuterium–helium-3 tandem-mirror generator — together with the intellectual-property estate, the people, and, in the internal edition, the full commercial case. The scientific text is the same text that appears in the arXiv preprints and the journal submissions; the editorial adds the apparatus a reader needs to hold the whole program at once, and nothing in the physics is altered to fit it.

THE HONESTY STANCE IS THE ASSET

Every headline quantity carries an **evidence class** — DERIVED RECOMPUTED MEASURED REQUIREMENT — and, where a number is a modelled extrapolation rather than a demonstrated value, it is labelled as such and its downside is shown next to it. Several quantities in the underlying corpus moved after first publication; where a value has been withdrawn or restated, the record says so plainly. This is deliberate: a diligence team will find the load-bearing assumptions, so the document surfaces them first.

TWO EDITIONS

This volume is issued in two editions. The **public edition** (light) carries the physics and the design only — no dollar, price, or per-kilogram figure appears anywhere in it. The **internal edition** (dark) adds the economics, the funding architecture, and the defense-commercial analysis, and is marked *Confidential* accordingly; it is not for public distribution. Where the commercial case rests on a modelled assumption rather than a demonstrated one, it is labelled as such and its downside is shown alongside it, on the same terms as the physics.

TITLE	The Kronos Fleet — Hyperion · Aegis · MetroVolt: A Combined Design & Commercialization Study
AUTHOR	Priyanca Ford, Founder & CEO, on behalf of Kronos Fusion Energy
EDITION	2026 Combined Editorial · first issue
COMPANION WORKS	The five-paper arXiv drop — (1) Breeder, (2) Burner, (3) REBCO magnet & tape, (4) Direct Energy Conversion, (5) AI/ML/Quantum control — with matching numbered Zenodo deposits, plus the IOP journal and IAEA-FEC submissions. Patents were filed before the drop.
NAMING	Hyperion = the breeder; Aegis (defense) and MetroVolt (data-center) = one generator in two housings. Internal mode letters (D1, L) do not appear on public surfaces.
STATUS	Conceptual design & simulation study. Nothing herein is a construction commitment.

HOW TO READ THIS VOLUME

The fleet at a glance, and the way its numbers are marked

This volume opens with *Orientation*, presents the five research papers as a bound sequence, and closes with the *Apparatus*. *Foundations* sets out the three general results both machines rest on. *Paper One* is the Hyperion breeder; *Paper Two* the Aegis / MetroVolt generator; *Papers Three, Four and Five* are the enabling science — high-field REBCO magnets and tape, direct energy conversion, and the AI / ML / quantum control stack. A *Digital Twin & 3-D Model* part follows, then the *Environmental* profile. The *Economics* and levelized cost and the *Business Case* and diligence record appear in the internal edition only; the *Simulations* proof record and the Apparatus — patent portfolio, team, limitations, and sources — close both editions.

THE FLEET AT A GLANCE

	HYPERION	AEGIS	METROVOLT
Role	Strategic-isotope foundry	Defense installation power	Campus power
Machine	**Spherical tokamak**	**Tandem mirror**	**Tandem mirror**
Fuel	Deuterium–tritium	Deuterium–helium-3	Deuterium–helium-3
Delivers	Tritium · ^{3}He · 14 MeV n	Resilient installation power	Firm campus power
Physics bar	**Fusion gain only**	Closure (gates named)	Closure + lunar ^{3}He
In the fleet	Breeds the fuel	Proves the generator	Commercial destination

HOW THE NUMBERS ARE MARKED

Every headline quantity carries an evidence class — DERIVED from first principles, RECOMPUTED from raw data, MEASURED in hardware, or a REQUIREMENT yet to be met. Financial figures carry a case label and are confined to the internal (confidential) edition. Values that moved after first publication are shown as withdrawn or restated rather than quietly changed. A capability you can evaluate is one whose limits are on the page.

ABSTRACT

A Machine-Learning Interatomic-Potential to Activation-Transport Pipeline for Low-Activation Fusion Alloy Discovery: CHGNet Screening, DFT Confirmation, and OpenMC/FISPACT Down-Selection

Selecting a plasma-facing structural alloy for a fusion power plant is a search through a combinatorial composition space against two filters a human cannot apply by hand: thermodynamic stability and neutron activation. A refractory-alloy palette that is mechanically excellent but activates into a long-lived waste class is useless to a plant, and discovering this only after the mechanical case is built wastes the search. We formalise and reduce to practice a three-stage graphics-processing-unit (GPU) discovery pipeline that carries activation as a *first-class* filter, co-equal with stability, from the first stage. Stage one screens thousands of candidate compositions with a universal machine-learned interatomic potential (CHGNet), relaxing each to its ground state and ranking it by formation energy at near-density-functional accuracy but three orders of magnitude faster; a single-phase body-centred-cubic (BCC) constraint reduces **3162** candidates to **2853** survivors. Stage two confirms the survivors at full accuracy with plane-wave density-functional theory (DFT, Quantum ESPRESSO); the confirmation matters, because the surrogate is found to run systematically $0.1\text{–}0.3\ \mathrm{eV\ atom^{-1}}$ over-bound and to swap the first-wall/direct-energy-converter stability ordering, and DFT re-bases the strongly negative machine-learned ranking to a near-neutral, entropy-stabilised set (formation energies -0.015 to $+0.021\ \mathrm{eV\ atom^{-1}}$). Stage three down-selects the confirmed-stable set by neutron-transport-driven activation (OpenMC transport into a FISPACT/ALARA-class inventory calculation), rejecting any composition whose 100-year waste class or decay heat is unacceptable regardless of its mechanics. On the clean $\{\mathrm{W, Ta, V, Ti, Cr}\}$ palette every component follows an intermediate-level-waste→low-level-waste→clearable trajectory with a long-lived fraction of exactly zero, while dirty Nb/Zr/Mo reference alloys remain intermediate-level waste at 100 years with a long-lived fraction of unity. The pipeline is the reusable contribution: it turns an intractable hand search into an automated funnel from thousands of candidates to a qualified handful, with activation enforced early rather than checked late. The alloys the pipeline produced are reported in companion papers; this paper reports and validates the method. Every headline quantity is a frozen anchor (invention #4, gate KX-L1-A4) in the Kronos Physics De-Risking Register.

Open-access deposit (code & data, CC BY 4.0): DOI 10.5281/zenodo.22645797 · Zenodo community *kronos_fusion_energy*. Explore it live: interactive 3-D model · physics validator.

Keywords: machine-learned interatomic potentials · CHGNet · density-functional theory · special quasirandom structures · activation transport · low-activation alloys · refractory high-entropy alloys · spherical-tokamak breeder

CONTENTS

Table of Contents

NOMENCLATURE

Symbols, units, and the names of things

Q	plasma (fusion) gain, P_{fus}/P_{aux}
Q_E	engineering gain, net electric out / recirculating in
H_{98}	confinement enhancement over the IPB98(y,2) scaling
Z_{eff}	effective ion charge
c_{ee}	electron–electron bremsstrahlung leading coefficient, 2.120022 (exact)
τ_E	energy confinement time
I_p	plasma current
R_0, a	major radius, minor radius
κ, δ	elongation, triangularity
β_N	normalized plasma beta (Troyon-normalized)
TBR	tritium breeding ratio
DEC	direct energy conversion
CF	plant capacity factor (availability)
FOAK / NOAK / BOAK	first / n^{th} / best of a kind
Hyperion	the ST breeder (internal: Mode D2)
Aegis	the generator, defense/installation housing (internal: Mode M)
MetroVolt	the generator, data-center housing (Mode M)

§ 1

Introduction

THE TWO-FILTER PROBLEM FOR A FUSION STRUCTURAL ALLOY

A structural alloy for the first wall, divertor and direct-energy-converter (DEC) electrodes of a compact spherical-tokamak breeder must satisfy two independent hard filters that are rarely satisfied together. It must be *thermodynamically viable* — a single-phase solid solution, or at least a metastable one that does not decompose in service — and it must be *low-activation*, so that after a plant lifetime under 14 MeV neutron loading it decays to a manageable waste class within a human-relevant time rather than producing a long-lived, high-level-waste tail. The design point that anchors this study is the Hyperion breeder (major radius $R_0 = 1.20\,m$, aspect ratio $A = 2.5$, toroidal field $B_0 = 8\,T$, elongation $\kappa = 2.0$, negative triangularity $\delta = -0.30$, plasma current $I_p = 9.66\,MA$, fusion gain $Q = 3.076$, fusion power $P_{\text{fus}} = 85.04\,MW$, centrepost peak field 16.84 T) [1], a strategic-materials machine whose value proposition rests on producing tritium, helium-3 and 14 MeV neutrons without a long-lived activation legacy.

The composition space is enormous. A refractory high-entropy-alloy (RHEA) palette of five or more transition metals, each varied over a realistic concentration range, generates more candidate compositions than any team can evaluate by density-functional theory (DFT) directly; and for fusion each candidate must pass not only a stability test but an activation test whose answer depends on the isotopic content of every element chosen. Searching that space by hand is impossible, and searching it with DFT alone is intractable: a single variable-cell relaxation of a disordered 16-atom supercell is already a substantial calculation, and there are thousands of compositions to consider. What is required is a method fast enough to screen thousands, accurate enough to be believed after confirmation, and strict enough to make activation a filter rather than an afterthought.

PRIOR ART

Three literatures meet in this pipeline. First, *machine-learned interatomic potentials* (MLIPs) have made near-DFT energy and force evaluation available at a tiny fraction of the cost. The idea of learning the potential-energy surface from a local atomic descriptor dates to the neural-network potentials of Behler and Parrinello [2] and the Gaussian-approximation potentials of Bart\'ok and co-workers [3]; the recent generation of *universal* graph-network potentials — trained across the periodic table on large first-principles databases — can relax an arbitrary crystal without a composition-specific fit. CHGNet [4], the charge-informed potential used here, and its relatives M3GNet and MACE [5] report formation-energy errors of a few tens of meV per atom on held-out first-principles data, which is why they have become the default front end for high-throughput screening. Second, *high-throughput first-principles databases and workflows* — the Materials Project [6], the Open Quantum Materials Database [7], AFLOW [8] and the `pymatgen` toolchain [9] — provide the reference energies and the automation that make a funnel possible, and machine learning is now routinely used to accelerate materials discovery [10,11]. Third, the *fusion low-activation materials* tradition [26,27,28] has long recognised that the choice of alloying elements sets the activation outcome: niobium, molybdenum, nickel and several others breed long-lived isotopes under a fusion spectrum and are excluded from reduced-activation designs, while the refractory/high-entropy-alloy route [20,21,22,23,24,25] offers high melting points and radiation tolerance if the palette can be kept clean.

THE GAP AND OUR CONTRIBUTION

Each of these literatures treats one filter. MLIP screening ranks by stability; activation studies classify a fixed alloy after the fact. What is missing — and what a fusion plant actually needs — is a single pipeline that applies both filters, in the right order, with activation promoted to a first-stage design constraint rather than a post-hoc audit, and with the surrogate's error budget honestly measured against the DFT it approximates. This paper contributes exactly that. We give (i) a formal statement of the discovery problem as constrained combinatorial optimisation, and the governing equations of each stage — the MLIP surrogate, the Kohn–Sham ground truth, the configurational-entropy stability criterion, and the coupled transport–inventory activation calculation (§2); (ii) the numerical formulation and the GPU high-performance-computing (HPC) campaign that ran it, naming every code and its problem scale (§3–4); (iii) the results, including the measured surrogate error, the DFT-confirmed near-neutral leads, and the activation down-select, in eight figures and four tables (§5); (iv) a quantitative comparison to the published MLIP and low-activation-materials literature (§6); and (v) one honest limitation — the surrogate's elemental-reference hull proxy is not a true convex-hull test, so the DFT confirm stage is load-bearing, not optional (§7). Every quantitative claim traces to a frozen result in the Kronos Physics De-Risking Register [31]; the serial identifiers (e.g. KX-L1-A4, BR-L2-A9, ENV-A2) are given inline so each number is auditable. The alloy *results* — the qualified leads and their full mechanical qualification — are reported in the companion low-activation-alloys papers [32,33,34]; this paper reports and validates the *method*.

§ 2

Governing equations and the formal problem

THE DISCOVERY PROBLEM

Let a candidate alloy be a composition vector $x = (x_1, \dots, x_n)$ on the simplex $\Delta^{n-1} = \{ x : x_i \geq 0,\ \sum_i x_i = 1\}$ over a fixed elemental palette $\mathcal{P} = \{\text{W, Ta, V, Ti, Cr, ...}\}$. The discovery task is to return the subset $\mathcal{Q} \subset \Delta^{n-1}$ of compositions that jointly satisfy a stability constraint and an activation constraint,

$$\mathcal{Q} = \Big\{ x \in \Delta^{n-1} \ : \ g_{\text{stab}}(x) \leq 0 \ \wedge \ g_{\text{act}}(x) \leq 0 \Big\},$$

where g_{stab} measures thermodynamic viability (single-phase formation energy relative to competing states) and g_{act} measures the activation penalty (long-lived specific activity or waste class after a reference irradiation). Equation (1) is the formal object the pipeline evaluates. Its difficulty is that g_{stab} requires a quantum-mechanical energy and g_{act} requires a neutron-transport and transmutation calculation, neither of which is cheap, and the palette that minimises g_{act} (light, short-activating elements) is not the palette that minimises g_{stab} (refractory, cohesive elements). The two constraints are in genuine tension, which is why both must be applied and neither can be inferred from the other.

STAGE 1: THE MACHINE-LEARNED SURROGATE

The energy of a relaxed configuration $\{ r_i\}$ is approximated by a message-passing graph network that sums a local, charge-informed energy density ε over atomic environments D_i,

$$E_{\text{MLIP}}(\{ r_i\}) = \sum_i \varepsilon\big(D_i; \theta\big), \qquad F_i = -\nabla_{ r_i} E_{\text{MLIP}},$$

with learned weights θ and analytic forces F_i from automatic differentiation of the network [4]. The surrogate is useful only inside a validated error band relative to the ground truth,

$$\big\| E_{\text{MLIP}} - E_{\text{DFT}} \big\| \ \leq \ \delta,$$

and one of the results of this paper is a *measurement* of δ for our alloy family rather than an assumption of it (§5.2). The stability score is the formation energy per atom against elemental references,

$$E_f(x) = \frac{1}{N}\Big(E_{\text{alloy}} - \sum_i x_i \, E_i^{\text{bulk}}\Big),$$

where E_{alloy} is the relaxed supercell energy of N atoms and E_i^{bulk} the energy per atom of element i in its reference bulk phase. Stage one evaluates equation (4) with E from the MLIP of equation (2) and applies the screening filter $g^{(1)}_{\text{stab}}(x) = E_f^{\text{MLIP}}(x) - E_f^{\text{cut}}$ together with a single-phase BCC-lattice acceptance test.

STAGE 2: THE KOHN–SHAM GROUND TRUTH

The survivors are recomputed with plane-wave DFT. The Kohn–Sham system [12,13] replaces the interacting electron gas by non-interacting particles in an effective potential,

$$\Big[-\frac{\hbar^2}{2m}\nabla^2 + V_{\text{ext}}(r) + V_H[n](r) + V_{\text{xc}}[n](r)\Big]\phi_i(r) = \varepsilon_i \, \phi_i(r),$$

with the electron density and Hartree potential closing the self-consistent loop,

$$n(r) = \sum_i |\phi_i(r)|^2, \qquad V_H[n](r) = \int \frac{n(r')}{| r - r'|}\, \mathrm{d}^3 r',$$

and the exchange–correlation term treated in the generalised-gradient approximation of Perdew, Burke and Ernzerhof [14]. The confirmed formation energy is equation (4) evaluated with the converged DFT total energies, $E_f^{\text{DFT}}(x)$, and the stage-two filter is $g^{(2)}_{\text{stab}}(x) = |E_f^{\text{DFT}}(x)| - \Delta_{\text{neut}}$, i.e. acceptance of a near-neutral formation energy within a band Δ_{neut} set by the configurational free energy below.

ENTROPY-STABILISED STABILITY CRITERION

A refractory high-entropy alloy need not have a negative formation *enthalpy* to be a stable single phase; the configurational entropy of mixing can carry it. The relevant object is the Gibbs free energy of mixing,

$$\Delta G_{\mathrm{mix}}(\mathbf{x}, T) = \Delta H_{\mathrm{mix}}(\mathbf{x}) - T\,\Delta S_{\mathrm{conf}}(\mathbf{x}), \qquad \Delta S_{\mathrm{conf}} = -k_B \sum_i x_i \ln x_i,$$

with $\Delta H_{\mathrm{mix}} \approx E_f^{\mathrm{DFT}}$ at 0 K. For an equiatomic quinary ($x_i = 1/5$), $\Delta S_{\mathrm{conf}} = k_B \ln 5 = 1.39 \times 10^{-4}$ eV atom^{-1} K^{-1}, so at a representative fabrication temperature $T \simeq 1800\,K$ the entropic term is $T\Delta S_{\mathrm{conf}} \simeq 0.25\,\mathrm{eV\,atom}^{-1}$. This dwarfs the near-neutral formation enthalpies confirmed in §5.3 ($+0.007$ to $+0.021\,\mathrm{eV\,atom}^{-1}$), so $\Delta G_{\mathrm{mix}} < 0$ and the single-phase solid solution is thermodynamically preferred. Equation (7) is therefore the precise sense in which a near-neutral DFT formation energy is a *pass*: it sets the acceptance band $\Delta_{\mathrm{neut}} \sim T\Delta S_{\mathrm{conf}}$ and identifies the design as entropy-stabilised rather than enthalpy-stabilised.

STAGE 3: ACTIVATION TRANSPORT AND INVENTORY

The activation filter couples a neutron-transport calculation to a transmutation–decay inventory. The angular neutron flux $\psi(\mathbf{r}, \mathbf{\Omega}, E)$ satisfies the steady linear Boltzmann transport equation,

$$\mathbf{\Omega}\cdot\nabla\psi + \Sigma_t\psi = \int_{4\pi}\int_0^{\infty} \Sigma_s(\mathbf{\Omega}' \to \mathbf{\Omega}, E' \to E)\,\psi\,\mathrm{d}E'\,\mathrm{d}\Omega' + \frac{\chi(E)}{4\pi}\,S,$$

solved by Monte-Carlo transport (OpenMC [29]) with the fixed 14 MeV source S normalised to $P_{\mathrm{fus}} = 85.04\,MW$. The resulting multigroup flux drives the coupled Bateman transmutation–decay equations for the nuclide inventory $N_j(t)$,

$$\frac{\mathrm{d}N_j}{\mathrm{d}t} = \sum_{k\neq j}\Big(\lambda_{k\to j} + \bar{\sigma}_{k\to j}\,\phi\Big)N_k - \Big(\lambda_j + \bar{\sigma}_j\,\phi\Big)N_j,$$

with decay constants λ, spectrum-averaged transmutation cross-sections $\bar{\sigma}$ and scalar flux $\phi = \int\psi\,\mathrm{d}\Omega\,\mathrm{d}E$, integrated by a FISPACT/ALARA-class inventory solver [30]. The activation penalty is read from the cooled inventory as the specific activity and the regulatory waste-class index,

$$A(t) = \sum_j \lambda_j N_j(t), \qquad \mathrm{WDR}(t) = \sum_j \frac{C_j(t)}{C_j^{\mathrm{limit}}}, \qquad g_{\mathrm{act}}(\mathbf{x}) = \mathrm{WDR}(t_{100}) - 1,$$

where WDR is the waste-disposal rating (the sum of concentrations C_j normalised to their class limits, here NRC 10CFR61) and $t_{100} = 100$ the cooling-time endpoint. A composition passes stage three only if $g_{\mathrm{act}} \leq 0$, i.e. if it is at or below the accepted waste class at 100 years with an acceptable decay heat. The palette itself is the primary lever on g_{act}: excluding Nb, Zr, Mo, Hf and Al removes the dominant long-lived channels (Nb-94, Zr-93, Mo isotopes) before any transport is run.

§ 3

Numerical formulation

CONFIGURATION MODEL AND RELAXATION

Each disordered composition is represented by a 16-atom body-centred-cubic $2 \times 2 \times 2$ supercell with a seeded random (special-quasi-random-structure, SQS) decoration [18,19], so that the short-range order of the true random solid solution is approximated in a finite cell. The same seed (20260726) is used throughout so that the stage-1 and stage-2 cells are identical and the surrogate error of equation (3) is measured on matched geometries. In stage one the cell is relaxed on the MLIP potential-energy surface of equation (2) to a force/stress tolerance; in stage two the same cell is relaxed by variable-cell BFGS on the DFT surface. Formation energies are taken relative to CHGNet-relaxed elemental references in stage one and BCC elemental references in stage two, consistent within each stage.

PLANE-WAVE DFT DISCRETISATION AND CONVERGENCE

The DFT calculations use plane-wave pseudopotential theory (Quantum ESPRESSO `pw.x` [15,16]) with the PBE functional [14], a Monkhorst–Pack k-mesh [17] and variable-cell BFGS relaxation to force and stress tolerances. Convergence is demonstrated by the divertor lead (BR-L2-A9): the variable-cell relaxation converges in 12 ionic steps to a total energy $E_{\mathrm{final}} = -8118.06554$ Ry, a relaxation energy of $-0.0205\ \mathrm{eV\,atom}^{-1}$ below the ideal-Vegard SQS starting geometry (-8118.04145 Ry), and a formation energy of $+0.0156\ \mathrm{eV\,atom}^{-1}$ against BCC elemental references. Cross-validation against a second, independent solver gives $+0.0147$ and $+0.016\ \mathrm{eV\,atom}^{-1}$ — agreement to the third decimal place — and a tungsten BCC smoke test returns $-12.7625\ \mathrm{eV\,atom}^{-1}$, matching the tracker reference (-12.76). These are the numerical-fidelity checks that license the stage-2 formation energies used below.

TRANSPORT AND INVENTORY DISCRETISATION

The neutron-transport solution of equation (8) is obtained by Monte-Carlo particle tracking (OpenMC) with ENDF/B-VIII.0 cross-sections, tallied on a 175-group VITAMIN-J energy structure at the first wall and normalised to the design fusion power. The first-wall spectrum used for the alloy inventory has a total flux of $6.30 \times 10^{16}\ \mathrm{n\,cm^{-2}\,s^{-1}}$, of which $4.04 \times 10^{15}\ \mathrm{n\,cm^{-2}\,s^{-1}}$ lies above 10 MeV. The Bateman network of equation (9) is integrated over the irradiation and cooling schedule by the inventory solver; the reported inventory spans 315 rows across 20 nuclides per composition. The stage-3 model here is a single-spectrum, first-wall-flux inventory (its one caveat, §7); the full three- dimensional rigorous-two-step shutdown-dose mapping is carried in the neutronics companions [35,36].

§ 4

Computational methodology: the GPU HPC campaign

The entire pipeline was executed on the Kronos NVIDIA GPU HPC campaign (an A100/H100/A10 fleet), with the reduced-order and inventory post-processing on the in-house research node. The division of labour follows the funnel:

Stage 1 — CHGNet / `pymatgen`. The universal MLIP relaxations are GPU-accelerated; the network of equation (2) evaluates energy and forces for an N-atom cell in a single forward/backward pass, so thousands of candidate supercells are relaxed and ranked at a cost per candidate roughly three orders of magnitude below a plane-wave relaxation (figure 8). This is what makes screening the full palette feasible.
Stage 2 — Quantum ESPRESSO `pw.x`. The confirmed subset (tens of compositions) is relaxed by GPU-enabled plane-wave DFT. Each variable-cell relaxation is a self-consistent-field calculation of a 16-atom metallic supercell with a dense k-mesh; the GPU acceleration is what brings the confirm stage into a few-day turnaround rather than weeks.
Stage 3 — OpenMC → FISPACT/ALARA. The Monte-Carlo transport of equation (8) is history-parallel and maps naturally onto the fleet; the inventory integration of equation (9) is a stiff-ODE post-process on the research node. itemize
Reproducibility is built in: a fixed random seed (20260726) for every SQS decoration, a fixed cross-section library (ENDF/B-VIII.0), and frozen anchors in the register mean the pipeline is deterministic up to Monte-Carlo statistics. No result in this paper depends on wall-clock or cost figures, and none is reported; the compute is described only by the codes run and the problem scale.

§ 5

Results

The pipeline is shown as a whole in figure 1 and the stage-by-stage attrition in figure 3. Table 1 states the three stages, their tool, filter and scale.

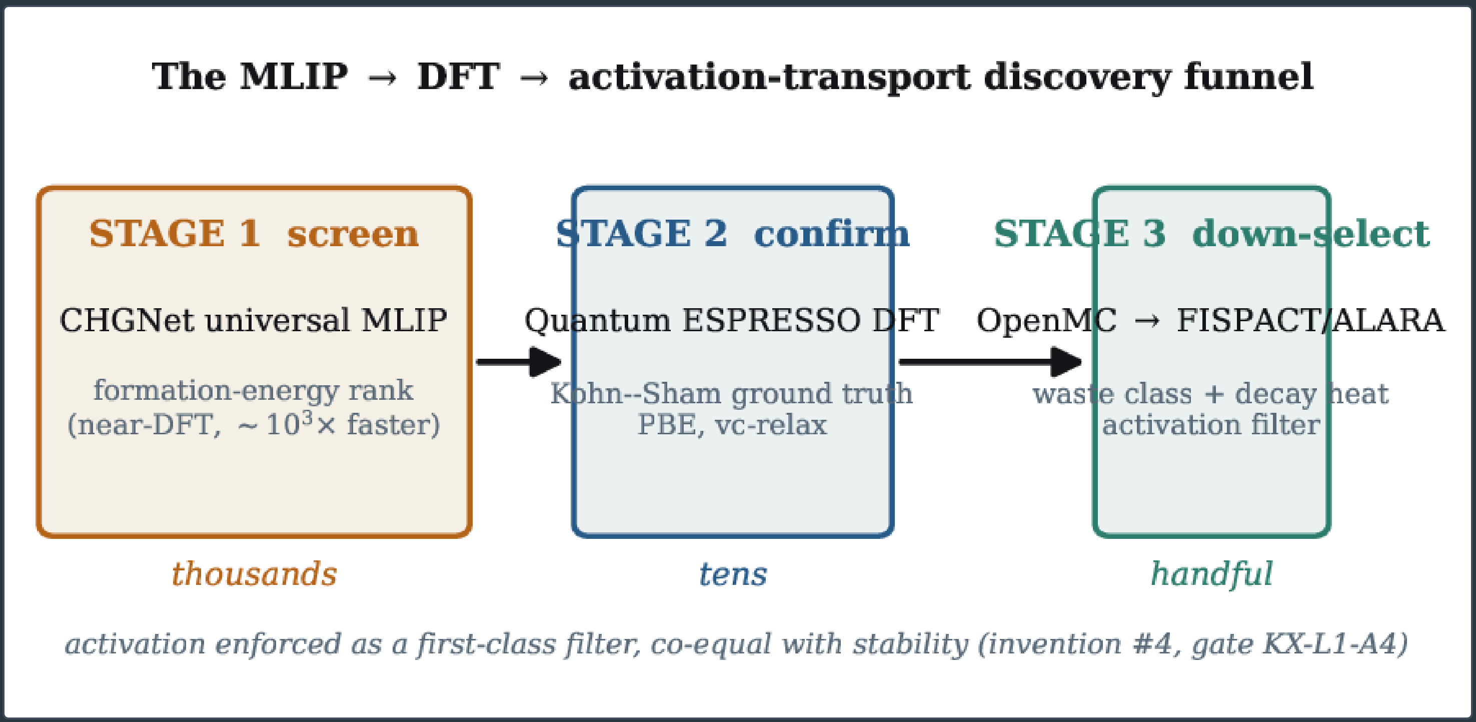

(Schematic.) The three-stage discovery funnel (invention #4, gate KX-L1-A4). A universal MLIP screens thousands of candidates by formation energy; DFT confirms tens at full accuracy; an OpenMC→ FISPACT/ALARA activation calculation down-selects to a qualified handful. Activation is a first-class filter, co-equal with stability. The figure encodes structure only; no data values are shown.

STAGE	TOOL (SERIAL)	FILTER	SCALE
1 screen	universal MLIP: CHGNet/`pymatgen` (KX-L1-A4)	formation energy + single-phase BCC	thousands
2 confirm	plane-wave DFT: Quantum ESPRESSO (BR-L2-A9)	near-neutral E_f at full accuracy	tens
3 down-select	OpenMC → FISPACT/ALARA (ENV-A2)	waste class + decay heat at 100 yr	handful

The materials-discovery pipeline (invention #4, gate KX-L1-A4). Serials refer to the register [31].

STAGE 1: THE MLIP SCREEN

The universal-potential screen ranks all candidate leads bound relative to elemental references (figure 2, KX-L1-A4/BR-L2-A8). The four primary leads relax to CHGNet formation energies of -0.393 eV atom^{-1} (blanket $Al_{50}Ti_{33}Zr_{10}Cr_7$), -0.286 eV atom^{-1} (divertor $Ta_{32}Re_{26}W_{18}Ti_{14}V_{10}$), -0.231 eV atom^{-1} (first wall $Ti_{47}W_{25}Fe_{20}Cr_8$) and -0.209 eV atom^{-1} (DEC $W_{48}Ti_{33}Cr_{10}Ta_4V_4$); the tantalum/rhenium-free A37 family holds together at -0.213, -0.174 and -0.126 eV atom^{-1}, so removing rhenium from the divertor lead costs only ~ 0.11 eV atom^{-1} of binding. A single-phase BCC-lattice test reduces the broader 3162-composition screen to 2853 single-phase survivors (figure 3; BR-SX-01). The MLIP thus does exactly its job: it discards the unstable majority cheaply and hands a ranked, bounded candidate set to the confirm stage.

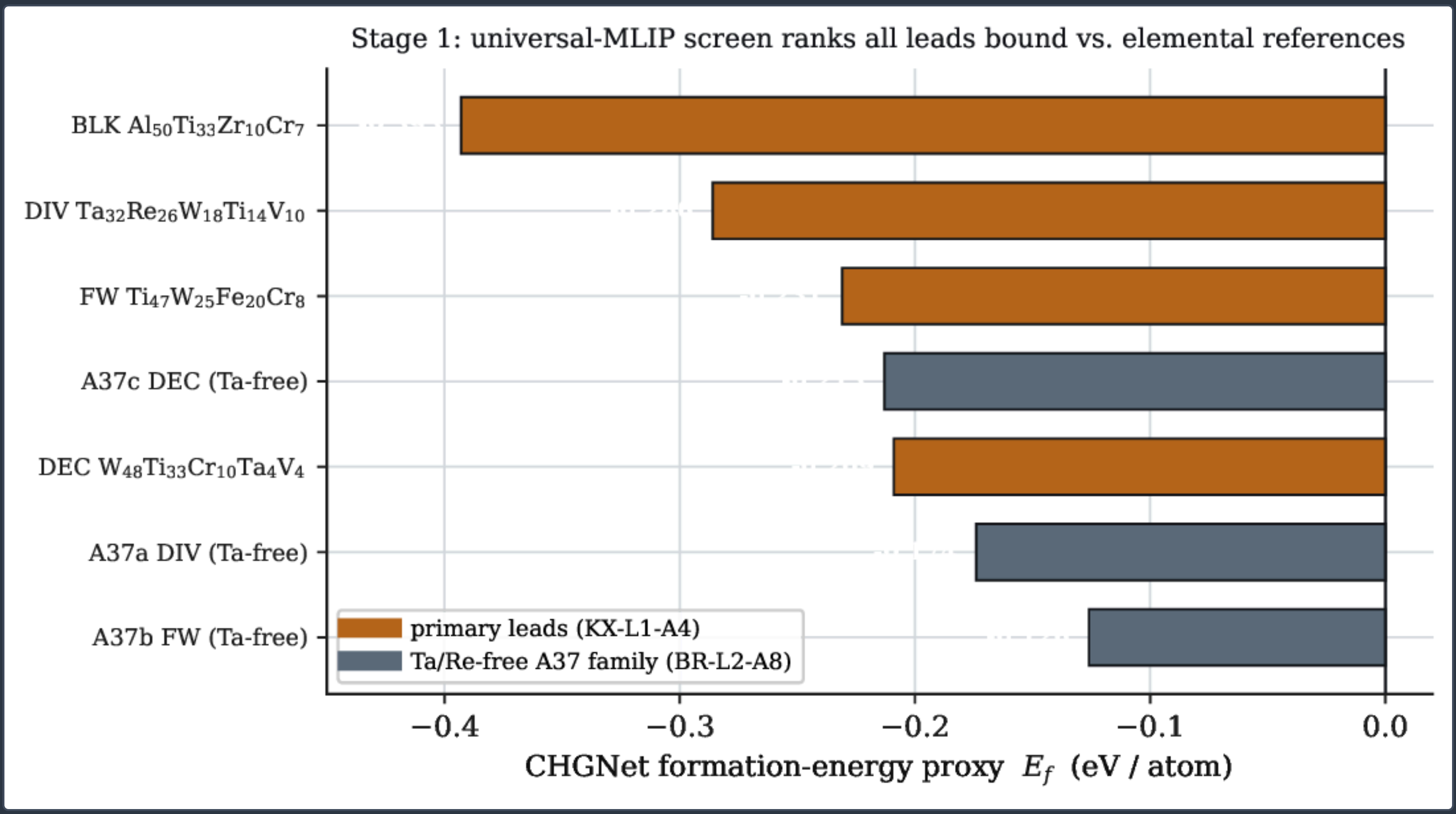

Stage 1 (data): CHGNet formation-energy proxy for the primary leads (KX-L1-A4) and the tantalum/rhenium-free A37 family (BR-L2-A8). All leads relax bound relative to elemental references. Values are register-frozen.

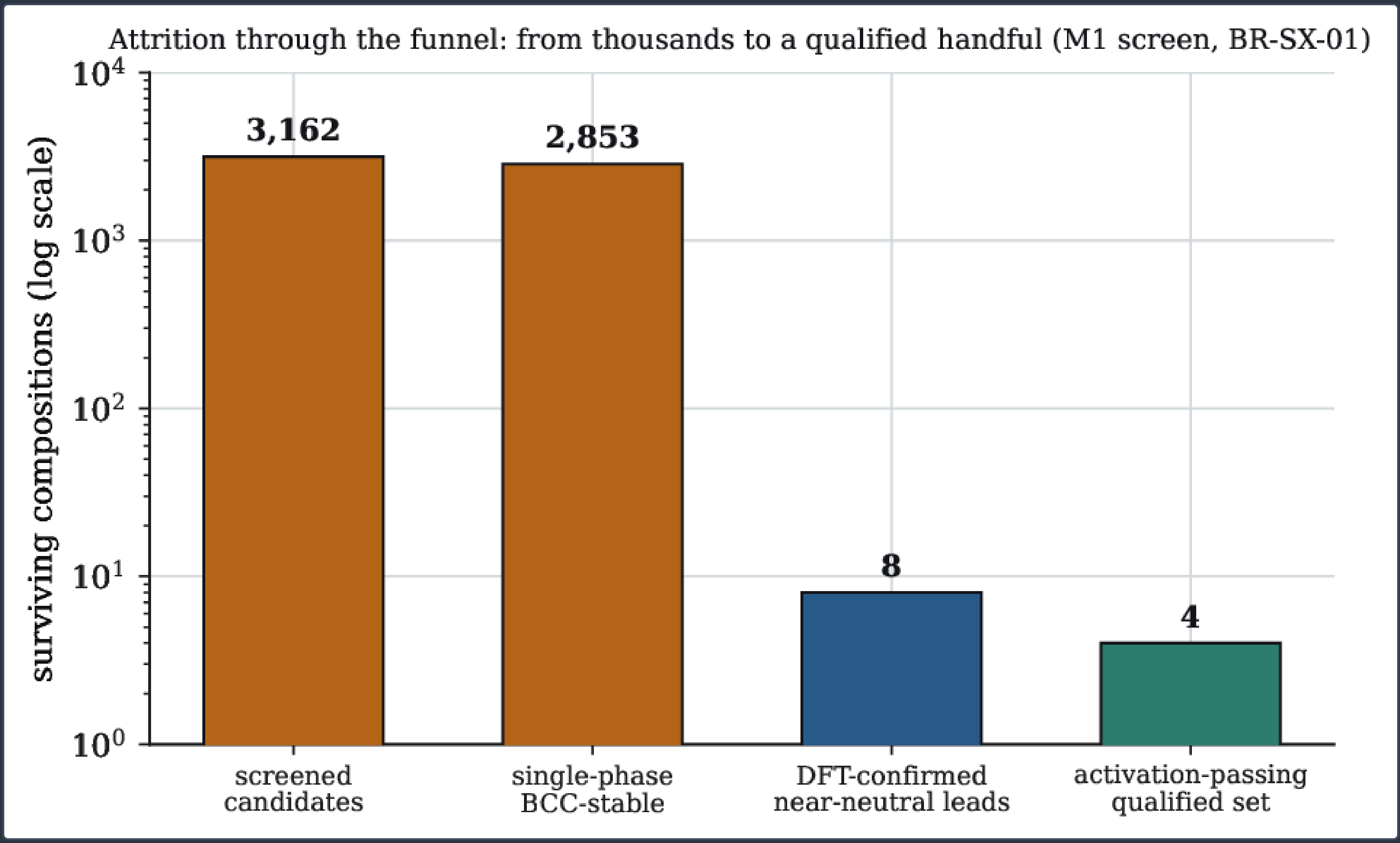

Attrition through the funnel (data): the M1 screen (BR-SX-01) reduces 3162 candidate compositions to 2853 single-phase BCC survivors; DFT confirmation returns of order ten near-neutral leads; the activation down-select qualifies a handful. The log ordinate makes the three-orders-of-magnitude reduction explicit.

THE MEASURED SURROGATE ERROR

The confirm stage is not a formality, and figure 4 is the reason. Comparing the CHGNet formation energies of the four screen families against their DFT values shows that the surrogate is systematically *over-bound*: every point lies well below the parity line, with the MLIP predicting formation energies 0.1–$0.3\ \mathrm{eV\ atom^{-1}}$ more negative than DFT (figure 4). Worse for a ranking method, the surrogate swaps the first-wall/DEC stability ordering: CHGNet places the first wall (-0.231) below the DEC ($-0.209\ \mathrm{eV\ atom^{-1}}$), whereas screen-grade DFT places the DEC (-0.028) below the first wall ($+0.090\ \mathrm{eV\ atom^{-1}}$). The offset is largest for the blanket lead ($-0.41\ \mathrm{eV\ atom^{-1}}$), which is Al–Ti intermetallic chemistry sitting off the BCC manifold the proxy assumes — a flagged case rather than a random error. This is a concrete, measured value of the surrogate bound δ of equation (3) for our alloy family, and it is exactly why a strongly negative MLIP ranking cannot be taken as a stability claim without DFT.

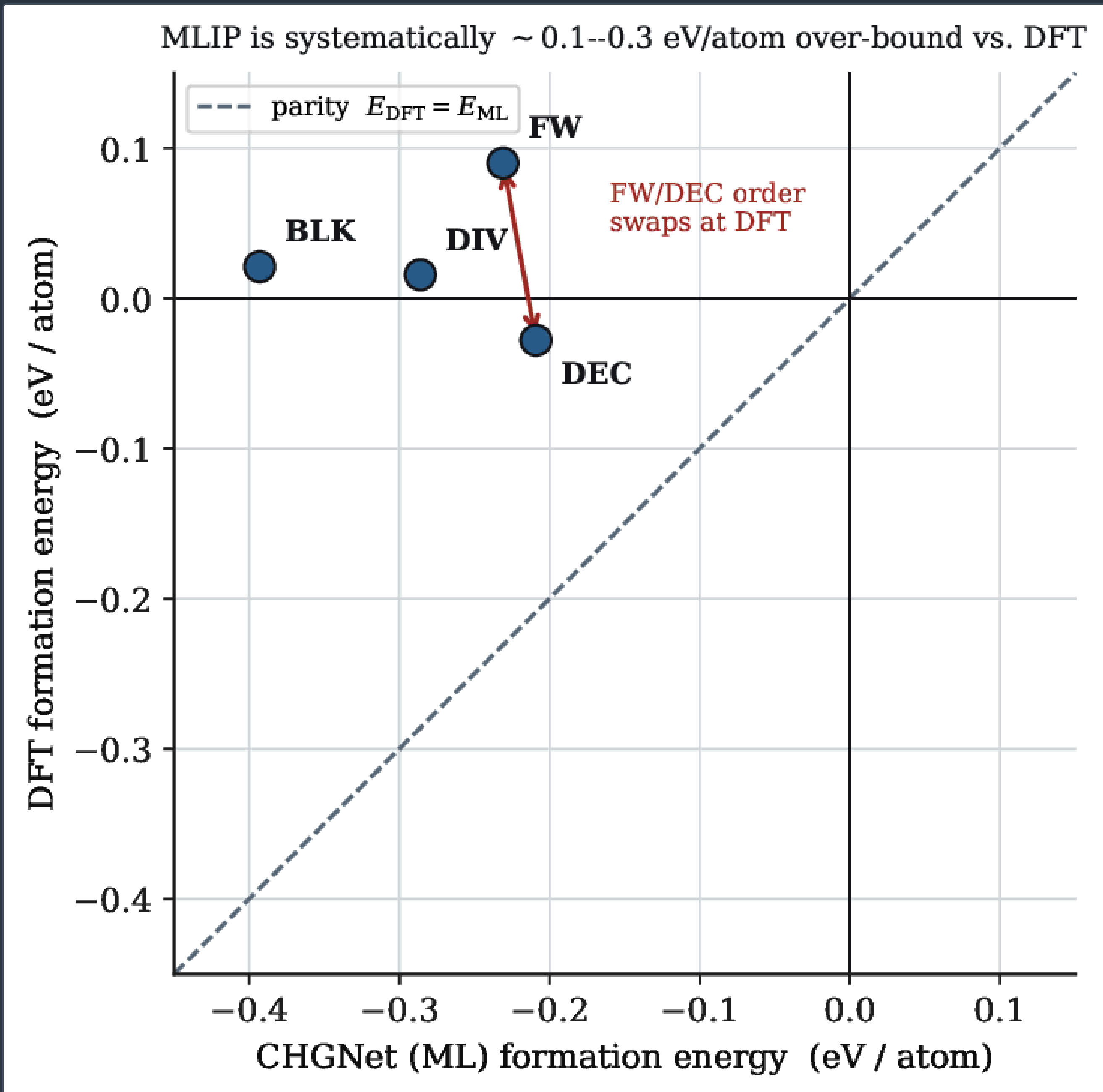
MLIP is systematically ~0.1--0.3 eV/atom over-bound vs. DFT
parity $E_{DFT} = E_{ML}$
FW
BLK
DIV
DEC
FW/DEC order swaps at DFT
0.1
0.0
−0.1
−0.2
−0.3
−0.4
DFT formation energy (eV / atom)
−0.4
−0.3
−0.2
−0.1
0.0
0.1
CHGNet (ML) formation energy (eV / atom)

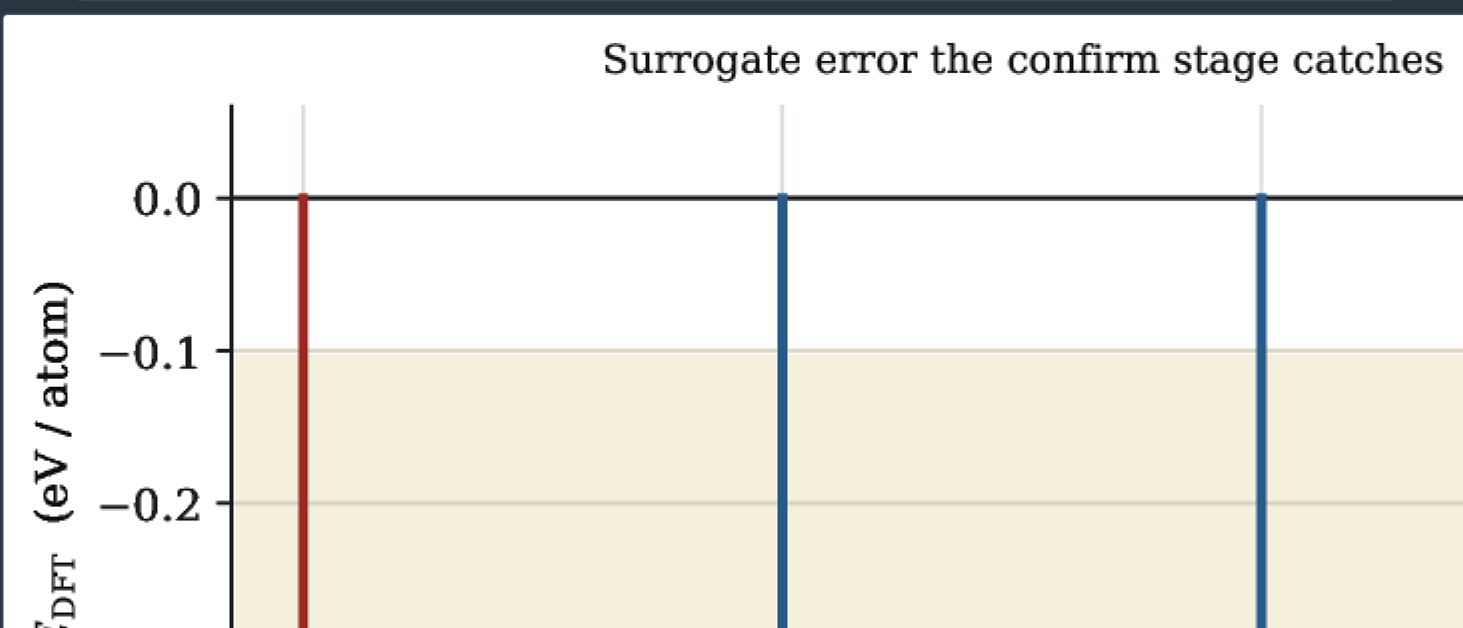
Surrogate error the confirm stage catches
0.0
−0.1
−0.2
(eV / atom)

STAGE 2: DFT CONFIRMATION RE-BASES THE LEADS TO NEAR-NEUTRAL

Full plane-wave DFT re-bases the strongly negative MLIP ranking to a near-neutral, entropy-stabilised set (figure 5, table 2). The confirmed 16-atom-SQS formation energies span $+0.021\ \mathrm{eV\,atom^{-1}}$ (blanket $Cr_3Ta_3Ti_3V_3W_4$), $+0.0156\ \mathrm{eV\,atom^{-1}}$ (divertor $Cr_1Ta_5Ti_3V_3W_4$), $+0.007\ \mathrm{eV\,atom^{-1}}$ (first wall $Cr_1Ta_4Ti_5V_3W_3$) and $+0.003\ \mathrm{eV\,atom^{-1}}$ (WTaVTi equiatomic, chromium-free), down to $-0.002\ \mathrm{eV\,atom^{-1}}$ (tantalum-free divertor and first-wall variants) and $-0.015\ \mathrm{eV\,atom^{-1}}$ (tantalum-free DEC $Cr_2Ti_5V_1W_8$). All are near-neutral within the acceptance band $\Delta_{\mathrm{neut}} \sim T\Delta S_{\mathrm{conf}}$ of equation (7); at a fabrication temperature of order 1800 K the configurational-entropy term ($\simeq 0.25\ \mathrm{eV\,atom^{-1}}$) exceeds every one of these formation enthalpies, so each lead is predicted to form a single-phase solid solution. The removal of tantalum, notably, does not cost stability — the tantalum-free A37 variants are as stable or slightly more stable than their tantalum-bearing parents — which is what allows the tantalum/rhenium-free family of the companion paper [33].

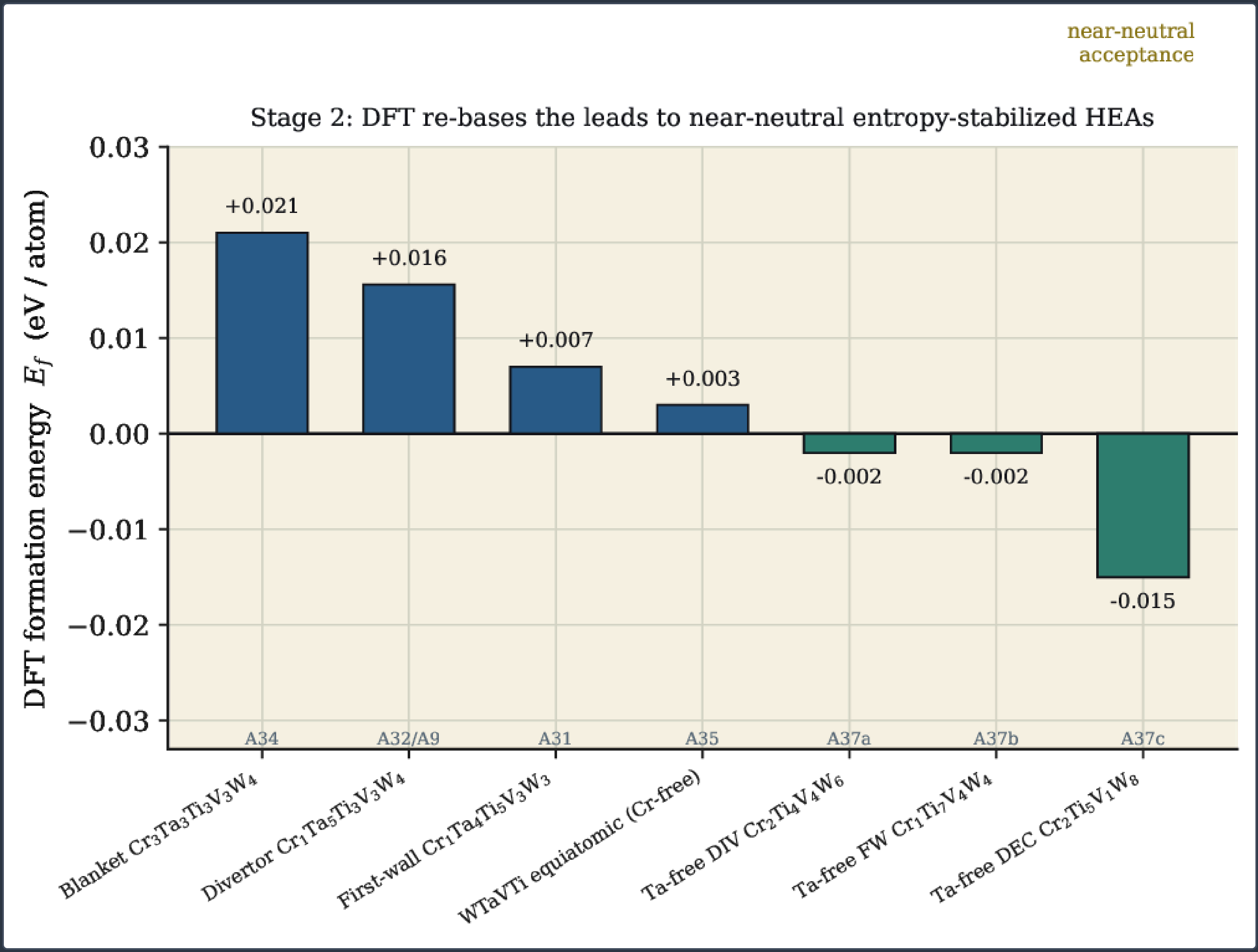

Stage 2 (data): DFT (Quantum ESPRESSO) formation energies of the confirmed 16-atom-SQS leads (BR-L2-A31/A32/A34/A35/A37a/b/c). The DFT values are near-neutral (shaded acceptance band), identifying the leads as entropy-stabilised high-entropy alloys rather than the strongly enthalpy-bound phases the MLIP suggested.

ROLE	COMPOSITION	E_f^{DFT} (eV atom^{-1})	SERIAL
blanket	$Cr_3Ta_3Ti_3V_3W_4$	+0.021	BR-L2-A34
divertor	$Cr_1Ta_5Ti_3V_3W_4$	+0.0156	BR-L2-A32/A9
first wall	$Cr_1Ta_4Ti_5V_3W_3$	+0.007	BR-L2-A31
refractory	WTaVTi equiatomic (Cr-free)	+0.003	BR-L2-A35
Ta-free divertor	$Cr_2Ti_4V_4W_6$	−0.002	BR-L2-A37a
Ta-free first wall	$Cr_1Ti_7V_4W_4$	−0.002	BR-L2-A37b
Ta-free DEC	$Cr_2Ti_5V_1W_8$	−0.015	BR-L2-A37c

DFT-confirmed formation energies of the **16**-atom-SQS leads (register serials in the last column). All are near-neutral; entropy stabilisation (eq. 7) carries them to a single-phase free energy at fabrication temperature.

STAGE 3: ACTIVATION DOWN-SELECT

The confirmed-stable set is then filtered on activation (figure 6, table 3; ENV-A2/BR-L1-A10). At the first-wall flux of 6.30×10^{16} n cm^{-2} s^{-1}, all four qualified HEA candidates follow the same trajectory: intermediate-level waste at 1 year cooling (total specific activity $\sim 6 \times 10^{14}$ Bq kg^{-1}, decay heat 51–62 W kg^{-1}), low-level waste at 10 years, and clearable at 100 years, with a long-lived fraction of exactly 0.0 at every cooling time. The dominant one-year inventory is short/medium-lived — W-181 (1.32×10^{15}), Ta-182 (1.17×10^{15}), W-185 (5.54×10^{14}) and Sc-46 (6.97×10^{13} Bq kg^{-1}) — so there is no long-lived tail. The full-chain ALARA classification of the actual first-wall and blanket components (BR-L1-A10) confirms the outcome at the plant level: every component is at or below NRC 10CFR61 Class C with no greater-than-Class-C (GTCC) material, the Class-C index staying $\leq 2.6 \times 10^{-3}$ in both zones at all times. The contrast cases make the point: dirty reference alloys containing Nb/Zr/Mo (REF_dirty_WTaNbMoV and REF_dirty_TiZrNbMoV) remain intermediate-level waste at both 10 and 100 years, with a long-lived fraction that rises to 1.0 (Nb-94, Zr-93, Mo isotopes). The clearable endpoint is bought by the palette choice, not by any post-processing.

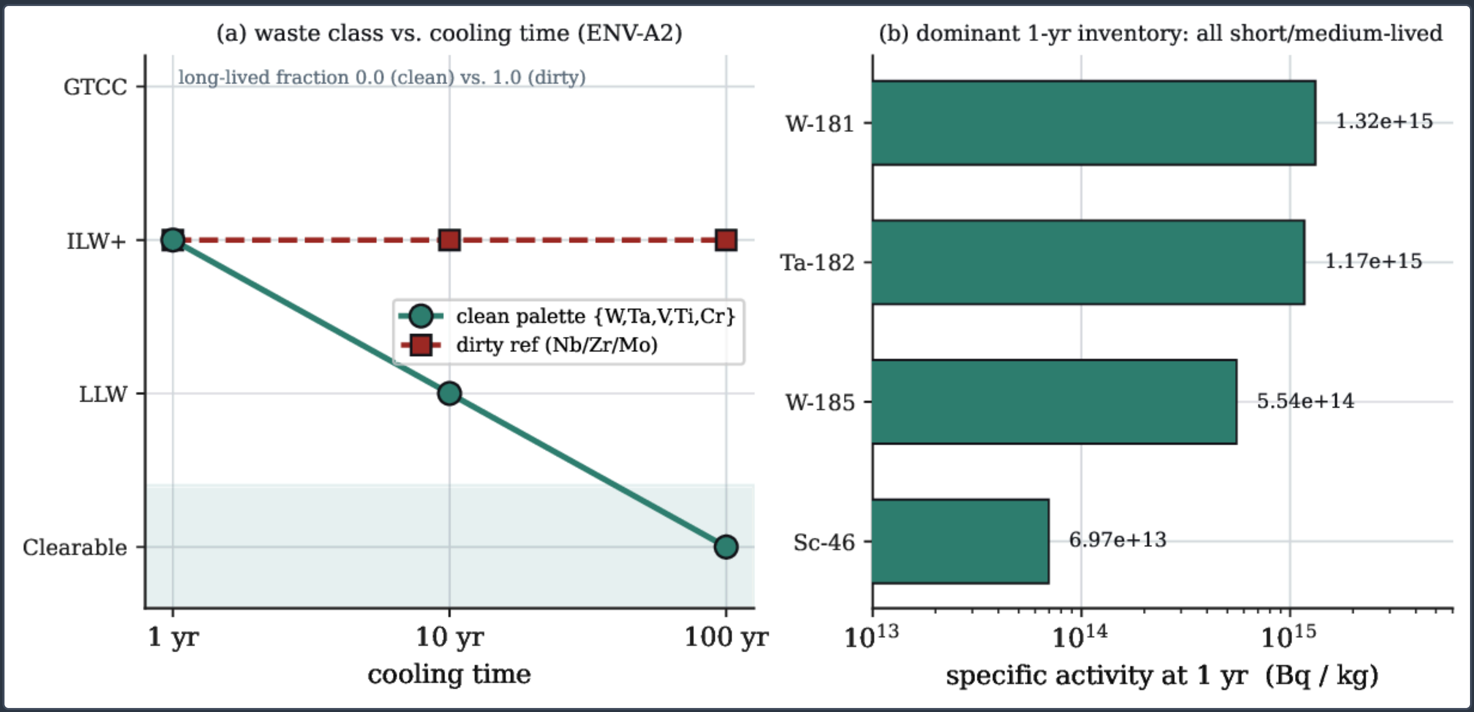

Stage 3 (data): the activation down-select (ENV-A2). **(a)** Waste class versus cooling time for the clean {W,Ta,V,Ti,Cr} palette (ILW→LLW→ clearable, long-lived fraction 0.0) against a dirty Nb/Zr/Mo reference (stays ILW+, long-lived fraction 1.0). **(b)** The dominant one-year inventory of the clean palette is entirely short/medium-lived.

MATERIAL	CLASS @ 1 YR	CLASS @ 10 YR	CLASS @ 100 YR	LONG-LIVED FRAC.
clean HEA {W,Ta,V,Ti,Cr}	ILW+	LLW	**clearable**	**0.0**
dirty WTaNbMoV	ILW+	ILW+	ILW+	1.0
dirty TiZrNbMoV	ILW+	ILW+	ILW+	1.0

Activation down-select of the clean-palette HEA family versus dirty references (ENV-A2/BR-L1-A10). Waste class at NRC 10CFR61; long-lived fraction from the cooled inventory.

THE JOINT ACCEPTANCE REGION

Figure 7 places the whole result in the plane the pipeline actually selects on: DFT formation energy on one axis, activation waste class on the other. The joint acceptance region — near-neutral formation energy ($|E_f| \le 0.05\ \mathrm{eV\ atom}^{-1}$) *and* waste class at or below low-level waste — contains the qualified leads and excludes the dirty references, which are thermodynamically comparable but activate into an intermediate-level tail. This is the crux the pipeline exists to enforce: a thermodynamically sound alloy is still rejected if its palette activates, and the rejection happens by construction rather than as an afterthought.

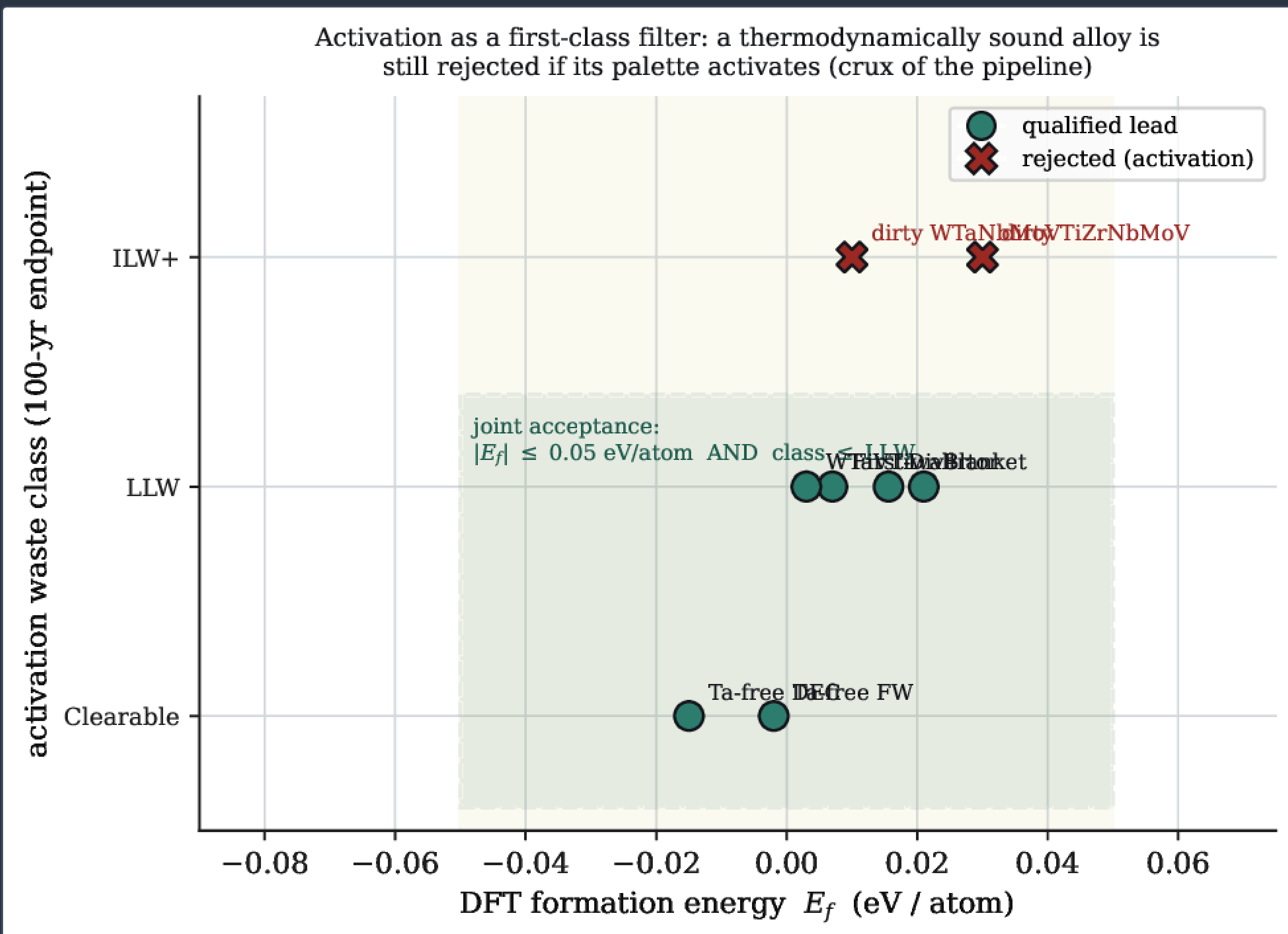

The joint acceptance region (data): qualified leads (circles) lie inside the near-neutral, class-≤-LLW box; dirty references (crosses) are excluded on activation despite comparable formation energies. Activation is a first-class filter, co-equal with stability.

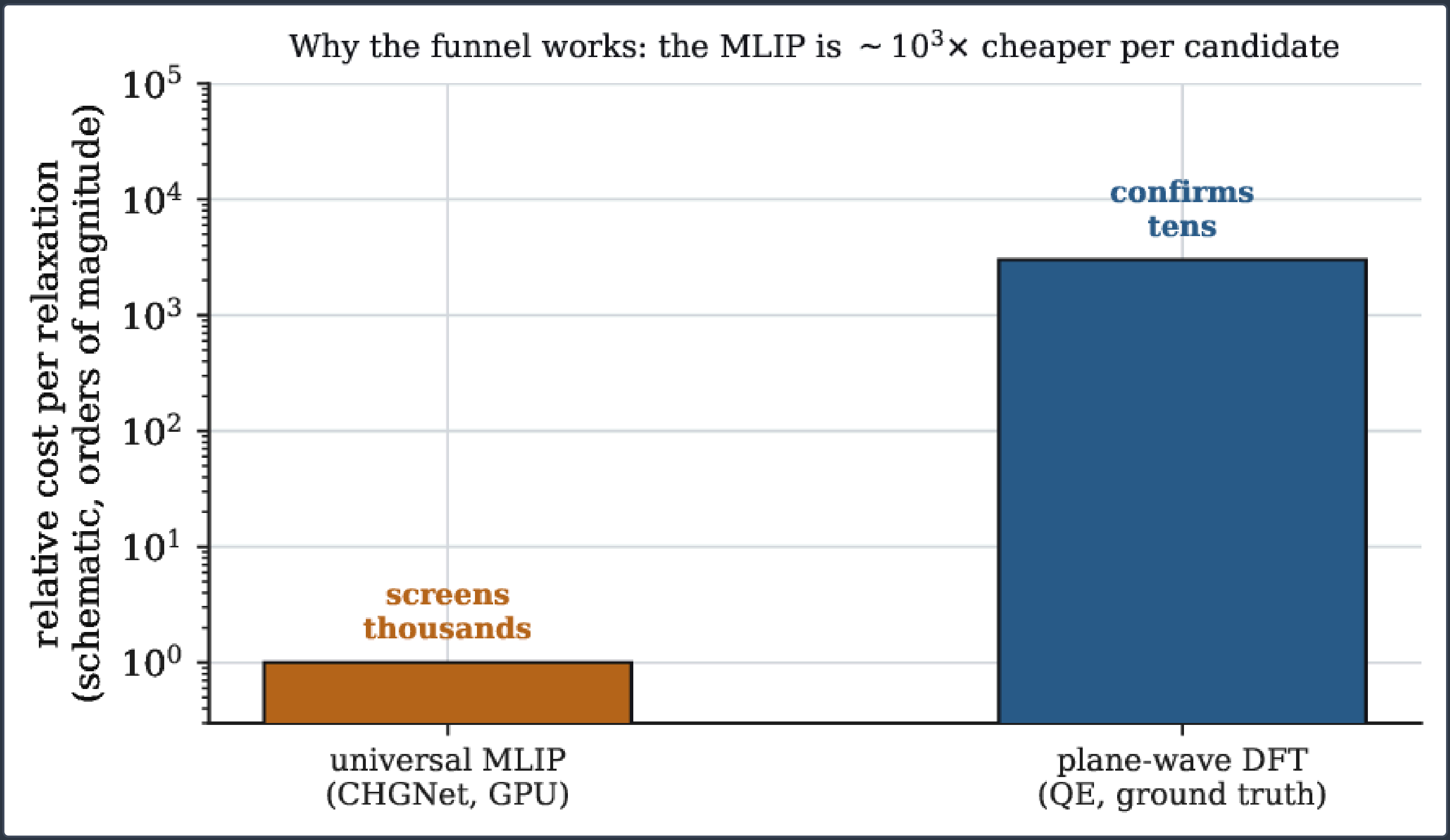

(Schematic.) Why the funnel works: the universal MLIP is roughly three orders of magnitude cheaper per relaxation than plane-wave DFT, so stage one can screen thousands where stage two confirms tens. Ordinate is a schematic order-of-magnitude cost per relaxation; no wall-clock or cost figures are implied.

§ 6

Discussion

THE SURROGATE ERROR AGAINST THE MLIP LITERATURE

The universal potentials that front this pipeline report formation-energy errors of a few tens of meV per atom on held-out first-principles data [4,5]. Our measured surrogate offset — 0.1–$0.3\ \mathrm{eV\,atom^{-1}}$, an order of magnitude larger — is not a contradiction but a statement about *what* is being compared. The literature error is a like-for-like energy MAE against the same DFT protocol and the same reference states; our offset is a formation energy computed against a hull *proxy* (elemental references only, no competing binaries or intermetallics) on a disordered 16-atom cell, and it mixes a genuine over-binding of the metallic solid solution with the failure of the BCC-lattice assumption for the Al-rich blanket composition (figure 4). The lesson is methodological and general: a universal MLIP used as a *ranking* front end inherits both its training-set accuracy and the systematics of the proxy it is scored against, so its ordering must be confirmed, not trusted — precisely the role stage two plays. When the confirmation is run, the qualitative screen conclusion (all leads bound, divertor most stable, tantalum removable) survives, while the quantitative magnitude is corrected from strongly negative to near-neutral. That the screen still points at the right region of composition space is the argument for the funnel; that it mis-states the magnitude is the argument for the confirm stage.

THE NEAR-NEUTRAL RESULT AGAINST THE LOW-ACTIVATION-MATERIALS LITERATURE

The DFT-confirmed leads are near-neutral rather than strongly stable, and this is the honest and physically correct picture for a high-entropy alloy: single-phase stability here is entropic, secured by equation (7) at fabrication temperature, not by a deep enthalpy well. This places the Kronos leads squarely in the refractory/high- entropy-alloy tradition [20,22,23,24,25], where configurational entropy is the stabilising agent and single-phase BCC solid solutions of refractory metals are the norm. On activation, the result is consistent with the established reduced-activation design rules [26,27,28]: the long-lived waste outcome is set by the elemental palette, and excluding Nb, Zr, Mo and their long-lived activation products is what buys the clearable endpoint. Our contrast cases quantify the rule directly — the identical alloy architecture with a dirty palette stays intermediate-level waste at 100 years with a long-lived fraction of unity, while the clean palette clears — which is the kind of controlled comparison that activation-ranking studies of fusion materials [30] call for. The novelty is not any single number but the placement of that number early in the search: the pipeline never spends its DFT budget on an alloy the activation filter will later reject.

RELATION TO A BEYOND-DFT CONFIRM STAGE

DFT itself is an approximation, and for the small formation energies at issue here the exchange–correlation functional is a real source of uncertainty. The natural extension is a higher-fidelity confirm stage — correlated quantum-chemistry or quantum-computed correlation energies for the same compositions — which the companion quantum-chemistry paper [37] pursues on a resource-honest basis. Within the present pipeline, the two-code agreement of §3 (QE $+0.0147$, second solver $+0.016\ \mathrm{eV\,atom^{-1}}$) bounds the numerical spread, and the uncertainty-quantification companion [38] places the alloy screen inside the broader design-plane error budget. None of these change the pipeline's logic; they refine the ground truth stage two rests on.

§ 7

Limitations

One honest gate bounds the stability claim. The stage-1 stability score is a formation energy against *elemental* references only — a hull proxy, not a true convex-hull test against competing binary and intermetallic phases — so it can misrank near-degenerate compositions and, for off-BCC chemistries such as the Al-rich blanket lead, mis-state the magnitude by up to $\sim 0.4\ \mathrm{eV\ atom}^{-1}$ (figure 4). This is exactly why the DFT confirm stage is load-bearing rather than optional, and why the confirmed formation energies are near-neutral: the honest current basis is that these leads are entropy-stabilised single-phase candidates within the acceptance band of equation (7), not deeply enthalpy-bound compounds. Two consequences follow. First, full thermodynamic qualification requires a finite-temperature free-energy calculation against competing phases and, ultimately, experimental single-phase confirmation — the open item, carried in the materials companions [32,33]. Second, the stage-3 activation model here is a single-spectrum, first-wall-flux inventory; the class boundaries would shift with the local spectrum, and the full three-dimensional rigorous-two-step calculation is carried in the neutronics companion [35]. Neither caveat weakens the method: the pipeline's value is that it surfaces both the surrogate error and the activation filter early, where they can steer the search, rather than late, where they would only invalidate it.

§ 8

Conclusion

A three-stage GPU pipeline — universal-MLIP screen, plane-wave-DFT confirmation, and OpenMC→ FISPACT/ALARA activation down-select — turns the intractable fusion plasma-facing-alloy search into an automated funnel from thousands of candidates to a qualified handful, with neutron activation enforced as a first-class filter co-equal with thermodynamic stability. The pipeline is validated end-to-end on the Kronos low-activation family: the MLIP screen ranks all leads bound and reduces 3162 candidates to 2853 single-phase survivors; the confirm stage measures a real surrogate error (0.1–$0.3\ \mathrm{eV\,atom^{-1}}$ over-binding, with a first-wall/DEC ordering swap) and re-bases the leads to a near-neutral, entropy-stabilised set (-0.015 to $+0.021\ \mathrm{eV\,atom^{-1}}$); and the activation down-select shows the clean $\{$W,Ta,V,Ti,Cr$\}$ palette clears to a zero long-lived fraction by 100 years while dirty Nb/Zr/Mo references do not. The reusable contribution is the method: a search that spends its DFT budget only on compositions the activation filter will accept, with the surrogate's error budget honestly measured rather than assumed. The alloys the pipeline produced, and their full mechanical and irradiation qualification, are the subject of the low-activation-alloys companions [32,33,34].

Acknowledgments tocsectionAcknowledgments Part of the Kronos Fusion Energy 2026 design series. The author thanks the Kronos physics de-risking programme for the frozen result set underlying every quantitative claim, and the reference open-source communities behind CHGNet, `pymatgen`, Quantum ESPRESSO, OpenMC and ALARA/FISPACT-II.

Reproducibility. Every headline quantity in this paper is a frozen anchor (invention #4, gate KX-L1-A4) in the Kronos Physics De-Risking Register [31] (doi:10.5281/zenodo.22133057): the CHGNet screen (KX-L1-A4/BR-L2-A8), the DFT confirmation (BR-L2-A9 and BR-L2-A31/A32/A34/A35/A37a/b/c) and the activation down-select (ENV-A2/BR-L1-A10). Each is regenerable from the archived simulator and the figure-generation script (`make_figs_2-51_mlip_pipeline.py`) deposited with this paper, under a fixed seed (20260726) and ENDF/B-VIII.0 cross-sections. This paper is archived at doi:10.5281/zenodo.22645797; official version: https://www.kronosfusionenergy.com/publications/ml-potential-materials-discovery-pipeline.html; its official version is at https://www.kronosfusionenergy.com/publications/ml-potential-materials-discovery-pipeline.html. No result depends on unpublished or proprietary data, and no economic content is part of the public deposit.

Data availability tocsectionData availability The CHGNet formation energies, the DFT-confirmed formation energies, the ML-versus-DFT parity data, and the activation trajectory used for figures 2–7 are archived with the deposit at doi:10.5281/zenodo.22645797 and trace to the register [31] by the serial identifiers cited inline. The figure-generation script transcribes only register-frozen values.

Competing interests tocsectionCompeting interests Provisional patent applications relating to aspects of this work (composition-of-matter and the discovery method) have been filed.

tocsectionReferences

APPARATUS

Portfolio, People & Record

The intellectual-property estate, the people who built it, the limitations that gate it, and the sources it rests on.

1	4	40	27
GRANTED PATENT	2026 PROVISIONALS	TEAM MEMBERS	2022 PROVISIONALS

INTELLECTUAL PROPERTY

The patent portfolio

The estate spans a granted high-field magnet patent, pending utility and 2026 provisional filings that map to the two products, a digital-twin control provisional, a registered trademark application, and the original 2022 provisional family. Every patentable disclosure in the five-paper arXiv drop was protected **before** publication: the breeder and burner provisionals were filed 1–2 August, and a publication-gap omnibus filing the evening before the drop swept up the DEC, plasma-control, and REBCO-winding matter of the three otherwise-unprotected papers. Patent numbers and application serials are matters of public record; claim scope is summarised, not reproduced.

GRANTED & PENDING UTILITY

US 12,009,112	High-field tilted graded-REBCO magnet architecture (KRONO-002A) · *app. 17/878,550*	GRANTED
US 17/878,507	Core device / method (KRONO-001A) · *utility*	PENDING

2026 PROVISIONAL FILINGS — MAPPED TO THE PRODUCTS

64/124,209	Hyperion — spherical-tokamak tritium / helium-3 foundry · *breeder · filed Aug 2026*	FILED
64/124,220	Aegis / MetroVolt — synchrotron-cutoff, fuel-selection & plug-winding · *generator · filed Aug 2026*	FILED
64/115,167	KRONOS-CTRL digital-twin plant control · *provisional · filed Jul 2026*	FILED
64/005,440	Integrated spherical-tokamak fusion architecture · *early integrated-architecture filing · filed Mar 2026*	FILED
64/105,530	Negative-triangularity spherical-tokamak architecture · *foundational ST filing · filed Jul 2026*	FILED
64/128,097	Publication-gap omnibus — quasineutral two-species expander DEC · provenance-gated / latency-split plasma control · as-built high-field winding & conductor architecture · *filed 7 Aug 2026, the evening before the arXiv drop*	FILED

TRADEMARK & ORIGIN

FTK-98801894	Kronos Fusion Energy — trademark application	FILED
KR-2022-*	Original provisional family (KR-2022-00001 … 00027) · *27 filings, 2022*	PRIORITY

The narrow, defensible magnet novelty — the specific conductor and the digital-twin winding optimisation, not high-field REBCO as a category — is the commercial core that can earn ahead of any Q > 1 milestone, with markets in fusion magnet supply, MRI/NMR, accelerators, and proton therapy. The claim is scoped honestly: the high field is a *system field* result, not a stand-alone-coil record; the small-bore plug coil is structurally infeasible as a bare winding but resolved by a stress-managed structural shield (feasible-pending-FEA); and the winding-tape experiment returned a *null result*. The value is the method, not a field record.

THE TEAM

Founding partners, board, advisors & auditors

Kronos is built by a bench of advanced-fuel-fusion, high-field-magnet, direct-conversion, and materials specialists, with a board and operations team drawn from defense, national laboratories, and industry. Dates are shown as ranges; where a tenure has ended or is term-ending, the range says so.

FOUNDING PARTNERS — SCIENCE

Dr. Gerald Kulcinski
Co-Founder · Helium-3 & Advanced-Fuel Fusion
UW–Madison · 2023–Present

Dr. Carl Weggel
Chief Scientist / S.M.A.R.T. Design
MIT Alcator Program · 2022–Present

Dr. Robert J. Weggel
Magnetic Field Design
MIT Magnet Lab · 2022–Present

BOARD

Priyanca Ford
Founder & CEO · Executive Board
2022–Present

Bandel Carano
Finance / Strategy
Oak Investment Partners / Stanford · 2025–2026

Patrick Schweiger
Fusion Device Engineering
Oklo / CFS / TerraPower · 2025–Present

SCIENTIFIC ADVISORS

Dr. Steven O. Dean
Fusion Policy & History
DOE / Fusion Power Associates · 2025–Present

Dr. Patrick H. Diamond
Plasma Turbulence & Transport
UC San Diego · 2025–Present

Dr. Jack J. Dongarra
HPC & Numerical Algorithms
Turing Award · 2025–Present

Dr. Nasr M. Ghoniem
Chief Material Scientist
UCLA · 2025–Present

Dr. Siegfried Glenzer
Plasma Physics & Laser Fusion
Stanford / SLAC · 2022–Present

Dr. David A. Hammer
Pulsed-Power Fusion
Cornell · 2025–Present

Dr. Donald A. Spong
Plasma Theory & Confinement
ORNL · 2025–Present

Dr. Curtis Smith
Risk Assessment & Nuclear PRA
MIT / Idaho National Lab · 2025–Present

RADM (Ret.) David Goggins
Naval Engineering & Power-Plant Design
U.S. Navy · 2023–2026

Dr. Konstantin Batygin
Mathematician
Caltech · 2022–2025

Dr. Ruben Fair
Magnet Design / ITER Liaison
PPPL / Jefferson Lab · 2022–2025

Dr. Paul S. Weiss
Materials & Nanotechnology
UCLA · 2022–2025

SCIENTIFIC AUDITORS

Dr. Wilfred A. Cooper
Plasma Equilibrium Theory
EPFL / Swiss Plasma Center · 2025–Present

Dr. Ahmed Hassanein
Plasma–Material Interactions
Purdue / Argonne · 2025–Present

Dr. Patrick E. Hopkins
Extreme Thermal Materials
U. of Virginia · 2025–Present

Dr. Peter Hosemann
Materials Joining & Structural Integrity
UC Berkeley · 2025–Present

Dr. Travis W. Knight
Advanced Nuclear Fuels & Systems
U. of South Carolina · 2025–Present

Dr. Philippe Lebrun
Cryogenics & Magnet Cooling
CERN · 2025–Present

Dr. Nitendra Singh
Nuclear Safety & Fuel Cycle
ITER · 2025–Present

Dr. Guido Van Oost
Magnetic Confinement & Fusion Systems
Ghent University · 2025–Present

Dr. Gary S. Was
Radiation Materials & Structural Integrity
U. of Michigan · 2025–Present

Dr. Ray Sedwick
Direct Energy Conversion
U. of Maryland · 2025

OPERATIONS

Michael Laughlin
Chief Operating Officer
2022–Present

Martin Owens
Chief Strategy Officer
LANL / GE Hitachi · 2022–Present

MG (Ret.) Paul Pardew
Chief Contracting Officer
Army Contracting Command · 2022–Present

David Beck
Fusion Commercialization
U.S. Space Force · 2024–Present

Sushma Bhatia
Environmental & Legislative
Google · 2022–Present

Michael De Frenza
Technology Licensing
2023–Present

MG (Ret.) Robin L. Fontes
Cybersecurity & Defense
Army Cyber Command · 2022–Present

Vijay Gehani
Supply Chain & Components
INOX India · 2024–Present

Jon Michel Greenwood
IT & AI Infrastructure
Live Nation · 2023–Present

Brian C. O'Neill
National Security
CIA / ODNI · 2022–Present

Gen. (Ret.) Gustave F. Perna
DoD Liaison
Operation Warp Speed · 2022–2023

Andrea Romero
Marketing Lead
2022–Present

Legal counsel is retained; those roles are held on the internal roster and are not listed here.

SOURCES

References

1 P I Ford, *Hyperion as a strategic-materials platform: gain, tritium breeding, He-3 co-production, and 14 MeV neutron output from a compact spherical tokamak*, Kronos Fusion Energy 2026 series. doi:10.5281/zenodo.22645691. Official page: kronosfusionenergy.com/publications/breeder.html.

2 J Behler and M Parrinello, Generalized neural-network representation of high-dimensional potential-energy surfaces, *Phys. Rev. Lett.* **98** 146401 (2007). doi:10.1103/PhysRevLett.98.146401

3 A P Bart\'ok, M C Payne, R Kondor and G Cs\'anyi, Gaussian approximation potentials: the accuracy of quantum mechanics, without the electrons, *Phys. Rev. Lett.* **104** 136403 (2010). doi:10.1103/PhysRevLett.104.136403

4 B Deng, P Zhong, K Jun, J Riebesell, K Han, C J Bartel and G Ceder, CHGNet as a pretrained universal neural-network potential for charge-informed atomistic modelling, *Nat. Mach. Intell.* **5** 1031 (2023). doi:10.1038/s42256-023-00716-3

5 I Batatia, D P Kov\'acs, G N C Simm, C Ortner and G Cs\'anyi, MACE: higher-order equivariant message-passing neural networks for fast and accurate force fields, *Adv. Neural Inf. Process. Syst.* **35** (2022).

6 A Jain, S P Ong, G Hautier *et al*, Commentary: the Materials Project — a materials genome approach to accelerating materials innovation, *APL Mater.* **1** 011002 (2013). doi:10.1063/1.4812323

7 S Kirklin, J E Saal, B Meredig, A Thompson, J W Doak, M Aykol, S R\"uhl and C Wolverton, The Open Quantum Materials Database (OQMD): assessing the accuracy of DFT formation energies, *npj Comput. Mater.* **1** 15010 (2015).

8 S Curtarolo, G L W Hart, M B Nardelli, N Mingo, S Sanvito and O Levy, The high-throughput highway to computational materials design, *Nat. Mater.* **12** 191 (2013). doi:10.1038/nmat3568

9 S P Ong, W D Richards, A Jain *et al*, Python Materials Genomics (pymatgen): a robust, open-source Python library for materials analysis, *Comput. Mater. Sci.* **68** 314 (2013). doi:10.1016/j.commatsci.2012.10.028

10 K T Butler, D W Davies, H Cartwright, O Isayev and A Walsh, Machine learning for molecular and materials science, *Nature* **559** 547 (2018). doi:10.1038/s41586-018-0337-2

11 A Merchant, S Batzner, S S Schoenholz, M Aykol, G Cheon and E D Cubuk, Scaling deep learning for materials discovery, *Nature* **624** 80 (2023).

12 P Hohenberg and W Kohn, Inhomogeneous electron gas, *Phys. Rev.* **136** B864 (1964). doi:10.1103/PhysRev.136.B864

13 W Kohn and L J Sham, Self-consistent equations including exchange and correlation effects, *Phys. Rev.* **140** A1133 (1965). doi:10.1103/PhysRev.140.A1133

14 J P Perdew, K Burke and M Ernzerhof, Generalized gradient approximation made simple, *Phys. Rev. Lett.* **77** 3865 (1996). doi:10.1103/PhysRevLett.77.3865

15 P Giannozzi, S Baroni, N Bonini *et al*, QUANTUM ESPRESSO: a modular and open-source software project for quantum simulations of materials, *J. Phys.: Condens. Matter* **21** 395502 (2009). doi:10.1088/0953-8984/21/39/395502

16 P Giannozzi, O Andreussi, T Brumme *et al*, Advanced capabilities for materials modelling with Quantum ESPRESSO, *J. Phys.: Condens. Matter* **29** 465901 (2017). doi:10.1088/1361-648X/aa8f79

17 H J Monkhorst and J D Pack, Special points for Brillouin-zone integrations, *Phys. Rev. B* **13** 5188 (1976). doi:10.1103/PhysRevB.13.5188

18 A Zunger, S-H Wei, L G Ferreira and J E Bernard, Special quasirandom structures, *Phys. Rev. Lett.* **65** 353 (1990). doi:10.1103/PhysRevLett.65.353

19 A van de Walle, P Tiwary, M de Jong *et al*, Efficient stochastic generation of special quasirandom structures, *Calphad* **42** 13 (2013).

20 J-W Yeh, S-K Chen, S-J Lin *et al*, Nanostructured high-entropy alloys with multiple principal elements: novel alloy design concepts and outcomes, *Adv. Eng. Mater.* **6** 299 (2004). doi:10.1002/adem.200300567

21 B Cantor, I T H Chang, P Knight and A J B Vincent, Microstructural development in equiatomic multicomponent alloys, *Mater. Sci. Eng. A* **375–377** 213 (2004). doi:10.1016/j.msea.2003.10.257

22 O N Senkov, G B Wilks, D B Miracle, C P Chuang and P K Liaw, Refractory high-entropy alloys, *Intermetallics* **18** 1758 (2010). doi:10.1016/j.intermet.2010.05.014

23 E P George, D Raabe and R O Ritchie, High-entropy alloys, *Nat. Rev. Mater.* **4** 515 (2019). doi:10.1038/s41578-019-0121-4

24 D B Miracle and O N Senkov, A critical review of high-entropy alloys and related concepts, *Acta Mater.* **122** 448 (2017). doi:10.1016/j.actamat.2016.08.081

25 O N Senkov, D B Miracle, K J Chaput and J-P Couzini\'e, Development and exploration of refractory high-entropy alloys — a review, *J. Mater. Res.* **33** 3092 (2018).

26 E E Bloom, The challenge of developing structural materials for fusion power systems, *J. Nucl. Mater.* **258–263** 7 (1998).

27 S J Zinkle and G S Was, Materials challenges in nuclear energy, *Acta Mater.* **61** 735 (2013). doi:10.1016/j.actamat.2012.11.004

28 S J Zinkle and L L Snead, Designing radiation-resistance in structural materials for fusion energy, *Annu. Rev. Mater. Res.* **44** 241 (2014). doi:10.1146/annurev-matsci-070813-113627

29 P K Romano, N E Horelik, B R Herman, A G Nelson, B Forget and K Smith, OpenMC: a state-of-the-art Monte Carlo code for research and development, *Ann. Nucl. Energy* **82** 90 (2015). doi:10.1016/j.anucene.2014.07.048

30 J-C Sublet, J W Eastwood, J G Morgan, M R Gilbert, M Fleming and W Arter, FISPACT-II: an advanced simulation system for activation, transmutation and material modelling, *Nucl. Data Sheets* **139** 77 (2017). doi:10.1016/j.nds.2017.01.002

31 P I Ford, *Kronos Physics De-Risking Register*, v8, Kronos Fusion Energy 2026 series. doi:10.5281/zenodo.22133057

32 P I Ford, *First-principles near-neutral low-activation refractory alloys for fusion plasma-facing components: formation-energy screening and entropy-stabilized composition-of-matter design*, Kronos Fusion Energy 2026 series. doi:10.5281/zenodo.22645744. Official page: kronosfusionenergy.com/publications/low-activation-alloys.html.

33 P I Ford, *A tantalum- and rhenium-free low-activation alloy family for first wall, divertor and direct-energy-converter electrodes: a first-principles composition-of-matter study*, Kronos Fusion Energy 2026 series. doi:10.5281/zenodo.22645891. Official page: kronosfusionenergy.com/publications/a-tantalum-and-rhenium-free-low-activation-alloy-family.html.

34 P I Ford, *A radiation-tolerant refractory high-entropy alloy for fusion plasma-facing components: microstructural stability and a scalable processing route*, Kronos Fusion Energy 2026 series. doi:10.5281/zenodo.22645868. Official page: kronosfusionenergy.com/publications/a-radiation-tolerant-refractory-high-entropy-alloy-for-.html.

35 P I Ford, *Component activation, waste-class routing, and decommissioning of a low-activation compact spherical-tokamak breeder: no isotope beyond a century's half-life*, Kronos Fusion Energy 2026 series. doi:10.5281/zenodo.22645846. Official page: kronosfusionenergy.com/publications/component-activation-waste-class-routing-and-decommissi.html.

36 P I Ford, *First-wall and plasma-facing-component lifetime under 14 MeV loading: displacement damage, bubble swelling and erosion in a compact spherical-tokamak breeder*, Kronos Fusion Energy 2026 series. doi:10.5281/zenodo.22645774. Official page: kronosfusionenergy.com/publications/first-wall-neutron-damage-lifetime.html.

37 P I Ford, *Quantum chemistry beyond DFT for low-activation fusion alloys: ADAPT-VQE correlation energies for composition-of-matter screening with fault-tolerant resource estimates*, Kronos Fusion Energy 2026 series. doi:10.5281/zenodo.22645929. Official page: kronosfusionenergy.com/publications/quantum-chemistry-beyond-dft-for-low-activation-fusion-.html.

38 P I Ford, *Global sensitivity and uncertainty quantification across the breeder and burner design planes: a 40,000-sample Monte-Carlo ranking of the frozen anchors*, Kronos Fusion Energy 2026 series. doi:10.5281/zenodo.22645893. Official page: kronosfusionenergy.com/publications/global-sensitivity-and-uncertainty-quantification-acros.html.

COLOPHON

How this document was made

The Kronos Fleet — Combined Editorial, 2026 is set in **Fraunces** (display), **Gelasio** (text), and **IBM Plex Mono** (data & equations), carried forward from the Kronos editorial design system.

The figures are rendered at 300 dpi from the deposited generator scripts; the document is composed as a single self-contained file with embedded fonts and imagery, paginated to US Letter, and rendered to PDF through a headless Chromium engine in matched light and dark editions.

Every headline quantity carries an evidence class; withdrawn and restated values are marked as such. Nothing herein is frozen beyond the founder-approved Tier-A set.

Explore it live — turn the interactive 3-D model, run the deposited solvers in the physics validator, and watch the companion film series.

LEGAL NOTICE

Notice, status, and distribution

Conceptual design & simulation study. This document reports a conceptual design and simulation study. It is not a construction commitment, a safety-analysis report, a regulatory filing, or an offer of securities. Forward-looking statements — schedules, costs, market sizes, and performance — are estimates subject to the limitations set out in the Simulations part and may change.

Numbers and their classes. Quantities are reported with evidence classes and case labels; modelled, assumed, and requirement-class values are identified as such and are not to be quoted without their labels.

Public edition. This edition carries the physics and design only; all financial, funding, and defense-commercial content has been removed for public distribution. The scientific text corresponds to the arXiv and journal submissions.

THE 2026 KRONOS SERIES

One programme, many papers

This editorial is one paper in the Kronos 2026 series — a real fusion company's complete, reproducible physics record for a spherical-tokamak breeder and its low-neutron D–^{3}He tandem-mirror burners. Every headline number is a frozen anchor in the Physics De-Risking Register.

Explore the whole programme: the De-Risking Register, the interactive 3-D model, and the physics validator.

KRONOS FUSION ENERGY

A Machine-Learning Interatomic-Potential to Activation-Transport Pipeline for Low-Activation Fusion Alloy Discovery: CHGNet Screening, DFT Confirmation, and OpenMC/FISPACT Down-Selection

A real fusion company building real machines. Explore the science, live.

Zenodo · doi:10.5281/zenodo.22645797

Read on kronosfusionenergy.com

The Physics De-Risking Register